Western Washington University
Western CEDAR

Geology Faculty Publications

Geology

2010

Chemical Structure of Vanadium-based Contact Formation on n-AIN

S. Pookpanratana

R. France

M. Blum

Sean R. Mulcahy
Western Washington University, sean.mulcahy@wwu.edu

A. Bell

See next page for additional authors

Follow this and additional works at: https://cedar.wwu.edu/geology_facpubs

Part of the Physics Commons

Recommended Citation
Journal of Applied Physics 108, 024906 (2010); doi: 10.1063/1.3456060

This Article is brought to you for free and open access by the Geology at Western CEDAR. It has been accepted for inclusion in Geology Faculty Publications by an authorized administrator of Western CEDAR. For more information, please contact westerncedar@wwu.edu.

Authors
S. Pookpanratana, R. France, M. Blum, Sean R. Mulcahy, A. Bell, M. Bär, L. Weinhardt, Y. Zhang, T. Hofmann, O. Fuchs, W. Yang, J. D. Denlinger, T. D. Moustakas, and C. Heske

This article is available at Western CEDAR: https://cedar.wwu.edu/geology_facpubs/74

Chemical structure of vanadium-based contact formation on n-AlN

S. Pookpanratana, , R. France, , M. Blum, , A. Bell, , M. Bär, , L. Weinhardt, , Y. Zhang, , T. Hofmann, , O. Fuchs, , W. Yang, , J. D. Denlinger, , S. Mulcahy, , T. D. Moustakas, and , and C. Heske

Citation: Journal of Applied Physics **108**, 024906 (2010); doi: 10.1063/1.3456060
View online: http://dx.doi.org/10.1063/1.3456060
View Table of Contents: http://aip.scitation.org/toc/jap/108/2
Published by the American Institute of Physics

AIP | Journal of Applied Physics
Save your money for your research.
It's now FREE to publish with us -
no page, color or publication charges apply.
Publish your research in the
Journal of Applied Physics
to claim your place in applied
physics history.

JOURNAL OF APPLIED PHYSICS **108**, 024906 (2010)

Chemical structure of vanadium-based contact formation on n-AlN

S. Pookpanratana,[1,a)] R. France,[2] M. Blum,[1] A. Bell,[3] M. Bär,[1,4] L. Weinhardt,[5] Y. Zhang,[1] T. Hofmann,[1] O. Fuchs,[5] W. Yang,[6] J. D. Denlinger,[6] S. Mulcahy,[3] T. D. Moustakas,[2,b)] and C. Heske[1,c)]
[1]Department of Chemistry, University of Nevada, Las Vegas (UNLV), Las Vegas, Nevada 89154-4003, USA
[2]Department of Electrical and Computer Engineering, Boston University, Boston, Massachusetts 02215, USA
[3]Department of Geoscience, University of Nevada, Las Vegas, Las Vegas, Nevada 89154-4010, USA
[4]Solar Energy Research, Helmholtz-Zentrum Berlin für Materialien und Energie GmbH, 14109 Berlin, Germany
[5]Experimentelle Physik VII, Universität Würzburg, 97074 Würzburg, Germany
[6]Advanced Light Source (ALS), Lawrence Berkeley National Laboratory, Berkeley, California 94720, USA

(Received 17 May 2010; accepted 21 May 2010; published online 29 July 2010)

We have investigated the chemical interaction between a Au/V/Al/V layer structure and n-type AlN epilayers using soft x-ray photoemission, x-ray emission spectroscopy, and atomic force microscopy. To understand the complex processes involved in this multicomponent system, we have studied the interface before and after a rapid thermal annealing step. We find the formation of a number of chemical phases at the interface, including VN, metallic vanadium, aluminum oxide, and metallic gold. An interaction mechanism for metal contact formation on the entire n-(Al,Ga)N system is proposed. © *2010 American Institute of Physics*. [doi:10.1063/1.3456060]

I. INTRODUCTION

N-type $Al_xGa_{1-x}N$ alloys are of high interest due to their applications in optoelectronic devices, such as light emitting diodes,[1,2] lasers,[3] and photodiodes.[4] In such devices, forming Ohmic contacts is of large importance. However, this is a significant fundamental challenge for these materials. First, the electron affinity (χ) of GaN [χ=3.3 (Ref. 5) or 4.1 (Ref. 6)] and AlN [χ=1.9 (Ref. 5) or less than zero (Ref. 7)] are not conclusively known (but most likely very different), and the band gaps (E_g) of GaN (3.34 eV) and AlN (6.02 eV) (Ref. 8) are very different as well, and thus it is difficult to find *one* contact scheme compatible for the entire $Al_xGa_{1-x}N$ ($0 \leq x \leq 1$) alloy system. For these highly ionic semiconductors, the Fermi level of the metal does not appear to be pinned by surface/interface states of the semiconductor. Consequently, to form Ohmic contacts to AlN (and a variety of other semiconductors, such as n-ZnO or n-$SrTiO_3$), one needs to employ a metal with a very small work function,[9] e.g., VN. Vanadium-based contacts involving rapid thermal annealing (RTA) were first used on n-$Al_{0.3}Ga_{0.7}N$,[10] and it was found that Ohmic contact formation occurred at less severe conditions (i.e., lower processing temperatures) and similar properties when compared to the traditional Ti-based contacts used for n-$Al_xGa_{1-x}N$.[10,11] However, it was also found that, with increasing Al content in the alloy, the RTA temperature had to be increased for optimal specific contact resistivity.[11] Second, the employed contact schemes are very complex and empirically derived. Consequently, a deeper understanding of the underlying interface formation processes and insights into the character of interface species and secondary phases is lacking. Such understanding, however, is needed to further optimize the interfaces and thus performance of associated devices. While the motivation of this study is an applied one, the main goal of this work is to gain a fundamental understanding of the chemical interface processes during high-temperature annealing of such complex semiconductor–metal interfaces.

For a deeper insight into the interface properties, we have employed a unique combination of spectroscopic and microscopic tools. In particular, we have used x-ray photoelectron spectroscopy (XPS) and x-ray emission spectroscopy (XES) to study the local chemical environment at the surface and near-surface bulk in an atom-specific fashion. These techniques have previously been used successfully to shed first light on the V-based contact formation on n-GaN.[12] XES has also been widely used to investigate the electronic structure of GaN, AlN, and their alloys.[14–16] Here, XES was used to investigate the local atomic environment of nitrogen and vanadium of Au/V/Al/V/n-AlN structures before and after RTA treatment. Since XES is a photon-in-photon-out technique, it can probe the surface-near bulk and buried interfaces within the top tens to a few hundreds of nanometers. In addition, the surface composition before and after annealing was monitored by XPS. Furthermore, we have employed atomic force microscopy (AFM) in air to study the surface morphology before and after interface formation, and wavelength-dispersive x-ray spectroscopy (WDS) to investigate the lateral distribution (in the form of maps) of atomic species at the surface.

By combining the results from these complementary experimental approaches, we are able to depict a detailed model of the interface structure. As will be shown in Sec. III, this structure is very complex and indeed requires the combination of such fundamental and sophisticated techniques to gain a comprehensive picture.

a)Electronic mail: pookpanr@unlv.nevada.edu.
b)Electronic mail: tdm@bu.edu.
c)Electronic mail: heske@unlv.nevada.edu.

 © 2010 American Institute of Physics

II. EXPERIMENT

Si-doped AlN samples were grown by molecular beam epitaxy onto c-plane sapphire. Subsequently, metal layers were deposited by electron beam evaporation. Additional details of sample growth and preparation have been published elsewhere.[11] The Au/V/Al/V contact scheme (where Au is the topmost layer) consisted of Au(100 nm)/V(20 nm)/Al(80 nm)/V(15 nm) (all thicknesses given are nominal values). Samples were cut into two parts, one of which was RTA-treated (1000 °C for 30 s in N_2). The samples were then packed and sealed under dry nitrogen without air exposure (to minimize any external surface contamination) and shipped from Boston University to UNLV. Samples were unloaded without air exposure in an N_2-purged glovebox prior to direct transfer into the ultrahigh vacuum (UHV) chamber for XPS analysis. For the less surface-sensitive XES experiments, samples were briefly (<10 min) exposed to air prior to transfer into the UHV chamber at the Advanced Light Source (ALS). AFM experiments were conducted in air after completion of the XPS and XES experiments, and WDS was performed subsequently. Reference materials (VN powder, metal foils) were obtained from Alfa Aesar.

XES experiments were performed at Beamline 8.0.1 at the ALS, Lawrence Berkeley National Laboratory, in our solid and liquid spectroscopic analysis (SALSA) endstation.[17] SALSA is equipped with a high-resolution, high-transmission variable line spacing soft x-ray spectrometer (further details can be found elsewhere[18]). XPS experiments were performed at UNLV using a Mg K_α radiation x-ray source and a SPECS PHOIBOS 150MCD electron analyzer. The energy scale of the analyzer was calibrated using XPS and Auger lines of Au, Ag, and Cu.[19] AFM measurements were performed with a Park XE70 instrument in contact mode. Elemental WDS and backscattered electron (BSE) mapping was performed at the UNLV Electron Microanalysis and Imaging Laboratory with a JEOL JXA-8900 electron probe microanalyzer. The Au M_α, V K_α, and Al K_α fluorescence lines were detected simultaneously with three wavelength-dispersive spectrometers using lithium fluoride (for Au M_α and V K_α) and thallium acid phthalate (for Al K_α) analyzing crystals, an acceleration voltage of 20 kV at a beam current of 100 nA, and dwell time of 15 ms per pixel.

III. RESULTS AND DISCUSSION

In Fig. 1, N *K* XES spectra of an untreated and an RTA-treated sample are shown, along with n-AlN (epilayer) and VN (powder) reference spectra. The spectrum of the untreated sample was multiplied by 8000 to account for the significant x-ray attenuation in the metallic overlayers-the attenuation length (i.e., the film thickness that attenuates an x-ray beam to 1/e of its initial intensity) at 392 eV is 35 nm in Au, 323 nm in V, and 273 nm in Al.[20] This demonstrates the unique capability of XES to probe a buried system, even through a metal layer stack of a nominal thickness of 215 nm. The intensity of the N *K* XES spectrum after annealing is substantially increased due to morphological changes described below.

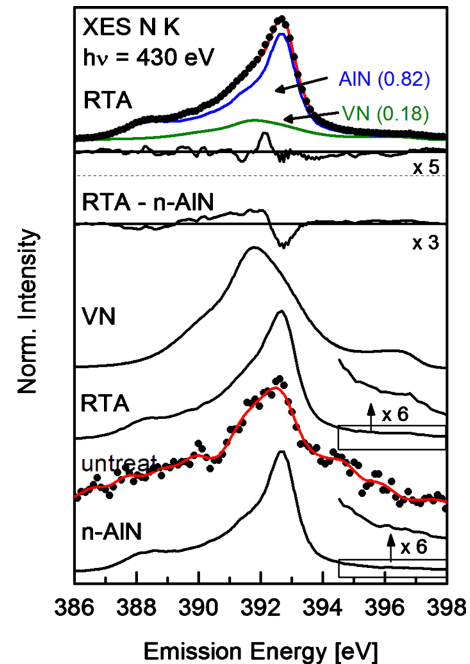

FIG. 1. (Color online) N *K* XES spectra of the untreated (data points and Fourier-smoothed curve) and RTA-treated (data only) sample, together with n-AlN and VN reference spectra. Above the VN spectrum, the difference (magnified) between the RTA-treated and the n-AlN spectrum (normalized to area) is shown. For the n-AlN and the RTA spectrum, an enlarged (×6) view of the uppermost valence band region is also shown. The top portion of the graph shows a fit (solid line) of the RTA-treated sample data (dots) using a sum of the n-AlN (82% area fraction) and VN (18% area fraction) spectra. The residual of the fit, magnified by a factor of 5, is also shown.

The energies of the main peak of the N *K* spectrum of both, the untreated and the RTA-treated sample, agree well with that of n-AlN. In fact, at first glance, the emission of the RTA-treated sample looks nearly identical to that of n-AlN but closer inspection reveals a slight shoulder at ~391 eV, best seen in the difference spectrum (RTA—n-AlN, magnified by 3) shown above the VN reference spectrum. This feature coincides with the main peak seen in the VN spectrum. To quantify the contributions from AlN and VN to the N XES spectrum, the spectrum of the RTA-treated sample is compared to a sum spectrum that was computed using the spectra of the n-AlN and VN references. This sum spectrum is also shown in Fig. 1 (top, red solid line), along with the measured data, the AlN and VN contributions, the residual (i.e., the difference between the data and the fit), and the utilized weight factors (which were determined with a least-square fit routine to minimize the residual). The result shows that $81 \pm 1\%$ of the peak area can be described with the n-AlN spectrum, and the rest ($19 \pm 1\%$) with the VN spectrum. Note that we do not attempt to interpret the line shape of the (very weak) peak of the untreated sample, since it is most likely obscured by background effects that can be neglected for all other (significantly more intense) peaks.

An additional indicator for the presence of VN in the RTA-treated sample is the observation of a "knee" at higher energies (~396–397 eV, see amplified region above the RTA spectrum). This feature is also present in VN but not in AlN, as can be seen from the amplified region shown above the n-AlN spectrum in Fig. 1. The feature is ascribed to

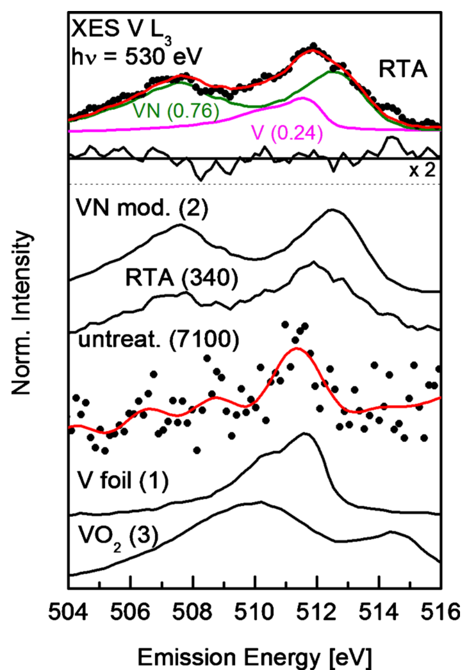

FIG. 2. (Color online) V L_3 XES spectra of the untreated (data points and Fourier-smoothed curve) and RTA-treated (data only) sample, together with V metal, VN, and VO_2 reference spectra. The VN spectrum is designated as modified ("mod."), because a vanadium oxide contribution was removed (for details see text). The top portion of the graph shows a fit (solid line) of the RTA-treated sample data (dots) using a sum of the V metal (24% area fraction) and the modified VN (76% area fraction) spectra. The residual of the fit is also shown, multiplied by 2.

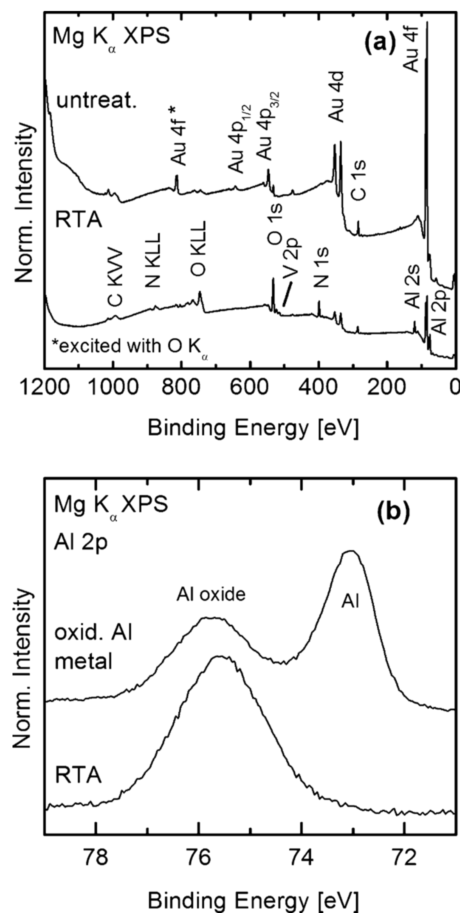

FIG. 3. (a) XPS survey spectra of the untreated and RTA-treated sample and (b) detail spectra of the Al 2p region of the RTA-treated sample and an oxidized Al metal foil.

valence electrons at and near the Fermi energy and their relaxation into the N 1s core hole (note that VN is considered to exhibit metallic character.[21–24] Thus, we conclude that the nitrogen atoms probed in the RTA-treated sample are present as AlN and partially transformed to VN as a result of the RTA treatment.

V L_3 XES suggests the formation of VN in the RTA-treated sample as well. The V L_3 spectra of the samples are shown in Fig. 2, along with a V metal, (modified) VN, and a VO_2 reference spectrum. For the VN reference (referred to as "VN mod."), we modified the spectrum of the as-received VN powder (Alfa Aesar) to account for the observed surface oxidation by subtracting a suitably weighted V L_3 spectrum of a VO_2 reference. The presence of VO_2 oxidation would add artificial spectral weight to the valley in VN (at approximately 510 eV). The weight was chosen based on the integrated area ratio for the O K emission in the VO_2 and the oxidized VN spectra (not shown) to approximate a "pure" VN spectrum.

The untreated sample has a V L_3 emission energy and broad shape similar to that of vanadium metal (as expected). The spectrum has a very low signal-to-noise ratio, since the V emission stems from atoms below at least (nominally) 100 nm of Au [the 1/e attenuation length at 510 eV in Au is about 43 nm (Ref. 20)]. Upon RTA treatment, the spectrum undergoes pronounced changes, most notably a substantial increase in intensity and an additional emission feature at lower energies. To understand the origin of this feature, a sum spectrum was computed using the VN (mod.) and V metal reference spectra and suitable weight factors to describe the RTA data (shown in Fig. 2, top portion). The weight factors were again determined with a fit, and it was found that the RTA spectrum can be best described with 76% (±5%) of the area from a VN (mod.) contribution, and 24% (±5%) from V metal. Thus, most of the probed V atoms exist in a VN environment, while some remain unreacted in a V metal environment. Note that we do not find any direct indication of the presence of vanadium oxide but small amounts might nevertheless be present (since there is some uncertainty in the "purity" of the VN mod. reference spectrum, as discussed above).

To summarize the XES results, we find the formation of VN as a result of the RTA treatment, and also detect the presence of metallic V and of AlN in the probed volume.

In order to complement these findings with very surface-sensitive information, the surface composition before and after RTA treatment was analyzed using XPS. Figure 3(a) shows the corresponding XPS survey spectra. As expected, the untreated sample surface is dominated by Au lines (i.e., from the topmost layer in the metal layer structure). Upon RTA treatment, the Au signals are significantly reduced, and previously buried elements (Al, V, and N) are now detected on the surface. This finding suggests significant interdiffusion processes and/or morphological changes as a result of the RTA treatment, which will be further discussed in the following paragraphs. We also note that, despite the efforts to

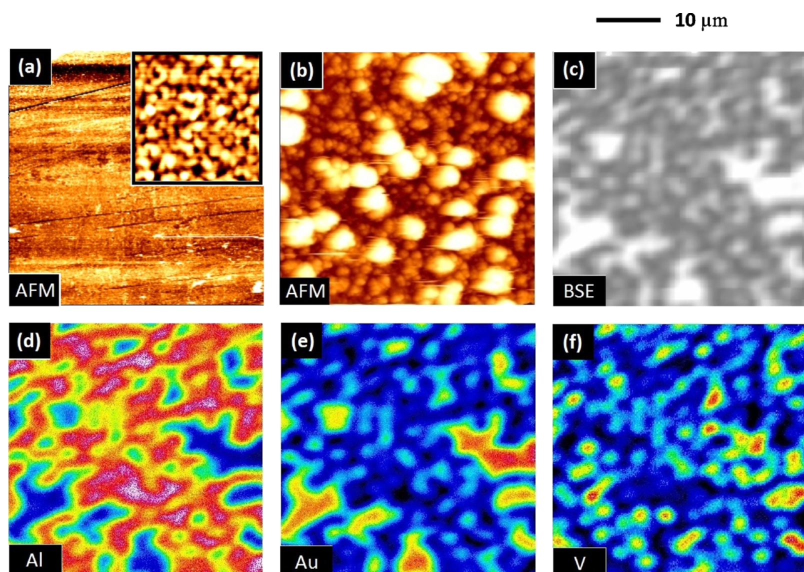

FIG. 4. (Color online) 40×40 μm^2 images of the untreated sample, acquired by (a) AFM (contact mode in air; inset shows a 1×1 μm^2 image), images of the annealed sample acquired by (b) AFM, (c) using backscattered electrons (BSEs), and (d)–(f) WDS. Images (c)–(f) were collected from the same location on the sample, while (b) was taken at a different location. The maximal AFM z-scale (elevation) between the dark (low) and white (high) areas is about 10 nm for (a) and about 1.4 μm for (b). The WDS maps show the elemental distribution (fluorescence intensity) of (d) Al, (e) Au, and (f) V. The intensity scale follows the colors of the electromagnetic spectrum-dark (online: black and blue): low; light (online: red and white): high.

minimize surface contamination (as described in Sec. II), both samples exhibit signals from C and O species on the surface. While the carbon signal is reduced after annealing, the oxygen signal is significantly enhanced, as evidenced by the increase in both the O 1*s* photoemission line as well as the O *KLL* Auger emission. Apparently, an oxide species has formed on the surface during the annealing step. In order to shed light on the chemical nature of the surface oxide, detail spectra were recorded for all metal lines observed in the survey spectra.

In Fig. 3(b), the Al 2*p* region is shown for the annealed sample and an oxidized Al metal foil reference (the Al foil was scratched in a N_2 filled glove box prior to transfer into UHV to also expose some metallic Al atoms at the surface). Note that the Al 2*p* feature was not detected in the untreated sample because of attenuation in the Au top layer.

Due to the Mg $K_{\alpha3}$ and $K_{\alpha4}$ excitation satellites of the (nonmonochromatized) x-ray source, the as-measured spectrum of the annealed sample has satellite contributions from the Au 4*f* lines in the Al 2*p* spectral window. To subtract these satellite lines, a sputter-cleaned Au reference foil was measured in the same energy window, and the spectrum was subtracted from the spectrum of the RTA-treated sample (after normalizing both spectra to the Au $4f_{7/2}$ main peak height). The result of this subtraction is shown in Fig. 3(b).

The oxidized Al metal reference foil has two components contributing to the Al 2*p* region—the feature at lower binding energies is due to metallic Al, while the one at higher binding energies is a native aluminum oxide, most likely Al_2O_3 (as it is thermodynamically most stable). The energetic positions of the two features are in agreement with the chemical shift reported between metallic Al and Al_2O_3 [+2.7 eV (Refs. 25–27) or +2.8 eV (Ref. 25)]. Note that the spin-orbit splitting between the $2p_{1/2}$ and $2p_{3/2}$ lines [0.4 eV (Ref. 28)] cannot be resolved in our measurements, since it is small compared to the experimental line width (dominated by the width of the excitation source) and likely further obscured by the presence of Al in (slightly) differing oxidation states.

As is apparent from the excellent agreement between the binding energy of the Al 2*p* peak of the annealed sample and the aluminum oxide peak of the Al reference foil, we find that the Al atoms at the surface are not metallic but exclusively in oxide form. This explains the significant increase in O 1*s* intensity; however, we note that, additionally, other oxides may exist. In particular, we cannot completely rule out the presence of some vanadium oxide—the peak position and line shape analysis of the V 2*p* photoemission and V *LMM* Auger lines is inconclusive, most likely due to the presence of both a VN and a metallic V species (in addition to a potential vanadium oxide).

To summarize the XPS findings, we note a significant change in surface composition after annealing, corroborating the XES-derived interpretation of significant interdiffusion processes and/or morphological changes as a result of the RTA treatment. We find a substantial reduction in the Au surface intensity, an increase in the V, Al, N, and O signals, and the clear presence of an aluminum oxide on the surface.

To supplement the compositional and chemical information derived from the spectroscopic data, we have collected contact-mode AFM images [Figs. 4(a) and 4(b)], a BSE image [Fig. 4(c)], and WDS elemental maps of Al, Au, V [Figs. 4(d)–4(f)] to derive the surface morphology and lateral elemental distribution. The AFM images of the untreated sample [Fig. 4(a)] exhibit a very flat surface (maximum elevation about 10 nm), covered with closely packed grains (with typical diameter of 100 nm), as expected for a thick metal overlayer and in agreement with the XPS information. In contrast, the surface of the annealed sample in Fig. 4(b) is rough (maximum elevation about 1.4 μm), with an inhomogeneous lateral distribution of large clusters (approximately 7 μm in diameter) and small clusters (approximately 1–2 μm in diameter) in-between. In the vertical dimension, the large clusters are about 1.4 μm higher than the lowest (darkest) regions. For the small clusters, this height is about 270 nm from the lowest regions.

The BSE map in Fig. 4(c) shows a similar structure, albeit at a different location on the sample. At the “BSE location,” the WDS maps show that the large clusters are mostly composed of Au [Fig. 4(e)], with some contribution

of V [Fig. 4(f); this is most easily seen for the three pronounced clusters in the bottom left corner or the three clusters at the bottom right edge of the maps]. We note that the distribution of V is "spotty"—apparently, islands or subclusters containing V are formed. As is evident from the Al and Au maps [Figs. 4(d) and 4(e)], their distribution is anticorrelated—for example, the three clusters with high Au and (spotty) V intensity correspond to low intensities in the Al map. Note that the 1/e attenuation length of the Al K_α fluorescence used for this map is between 162 nm (in pure Au) and 480 nm (in pure V).[20] Thus, this finding suggests the absence of Al in the large clusters, while it does not rule out the presence of Al atoms *underneath* the large clusters, i.e., in the n-AlN substrate.

In combining the results from the various elemental, chemical, and topographic probes, we are now able to paint (propose) a comprehensive picture of the interface structure between the metal overlayers and the n-type AlN film after annealing. From the AFM images, we find that the contact layers transform from a nanocrystalline closed layer to a surface with two types of clusters ("large" and "small"). From the WDS elemental mapping, we find that the large clusters are mostly composed of Au with some inhomogeneous V enclosures or islands. From the XES analysis, we know that these V regions contain vanadium in both, a metallic and a VN-like environment. In contrast to the large clusters, the small clusters show a strong Al signal and minimal Au and V intensity. From the XPS analysis, we know that these Al atoms (at least those at the surface) are exclusively in an aluminum oxide environment. The (laterally integrated) XPS intensity analysis shows that annealing leads to morphological changes that allow previously buried elements (N, Al, and V) to be detected at the surface, and, as mentioned, the AFM images and WDS maps can then be used to correlate this information with laterally-resolved insights, as described above.

The findings are summarized in the schematic structure shown in Fig. 5. During the annealing process, the atoms of the metallic top layers become very mobile and diffuse to form a very different surface morphology. Au and V atoms migrate to form large clusters (with the V being present in both metallic and VN form), while Al atoms migrate to form small clusters, presumably forming an aluminum oxide, and leading to an increased number of grain boundaries. The effective overall thickness of the "cover layer" is thus reduced, so that, e.g., the AlN substrate becomes "visible" in XES. As mentioned, the XES analysis confirms the formation of VN as a result of the RTA treatment. For reasons discussed below, we speculate that the nitrogen source for this VN formation is likely the AlN layer, and that thus the VN is located at the interface between the large clusters and the AlN substrate. Also, note that the WDS maps show an inhomogeneous lateral V distribution within the large clusters (not shown in Fig. 5).

As mentioned, we propose that the nitrogen source for the VN formation is the AlN substrate (and not the ambient N_2 molecules during the RTA step). For n-GaN, we could previously show the presence of metallic Ga at the (Au, V, Al)/GaN interface, suggesting that the nitrogen source was indeed the GaN substrate.[12] In the present case, a similar experimental argument cannot be applied, since the Al signal is vastly dominated by the Al atoms in the AlN substrate, and because Al is additionally present in the (initial) contact scheme. France *et al.*[11] found that for optimal contact resistivity in the (Al,Ga)N alloy system, the required RTA processing temperature increases with increasing Al content—varying from 650 °C (pure n-GaN) to 1000 °C (pure n-AlN) and proposed that the formation of VN was directly involved with forming Ohmic contacts. It was hypothesized that the RTA temperature was related to the bond strength (E_b) of Ga–N and Al–N.[11] Indeed, Talwar *et al.*[29] report that $E_{b,Al-N} > E_{b,Ga-N}$. If we assume that ambient N_2 molecules serve as the nitrogen source for VN formation, then the processing temperature should be independent of alloy composition since the V–N interaction is independent of the underlying substrate material (GaN or AlN). Furthermore, if the nitrogen originated from the ambient, then the fraction of VN detected in V $L_{2,3}$ XES should be constant when compared to the metallic V emission (for both GaN or AlN substrates since the contact schemes are identical). In contrast, we find (here, and in Ref. 12) that the fraction of VN detected is not the same for the AlN and GaN systems. Since the optimal RTA processing temperature is reported to be dependent on the (Al,Ga)N composition, it is thus very unlikely that the ambient N_2 plays a significant role as a nitrogen source. In contrast, this analysis suggests the n-(Al,Ga)N alloy as the nitrogen source for VN formation, as in the case of n-GaN.[12]

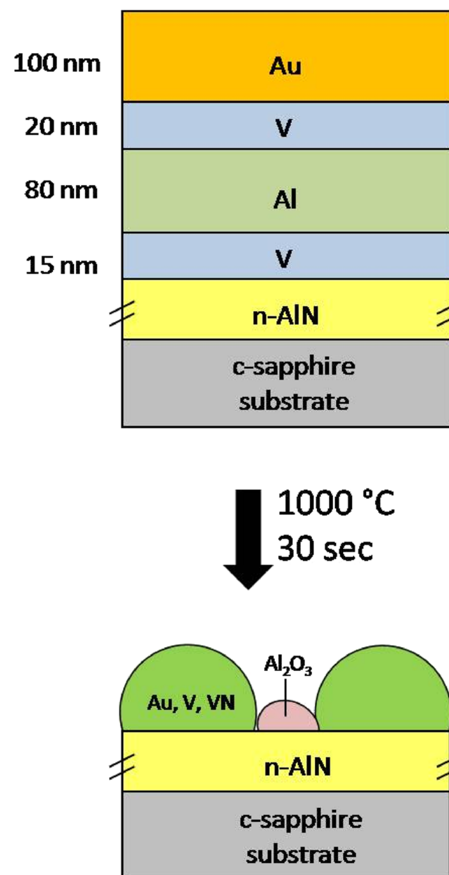

FIG. 5. (Color online) Schematic of metal/n-AlN contact structure before and after RTA.

These findings shed light on the fundamental interactions between metal contact layers and the n-(Al,Ga)N alloy system during annealing. The N *K* XES spectra of n-GaN show the nitrogen atoms in a dominant VN chemical environment,[12] while for n-AlN, the N is dominant in an AlN environment with some VN contributions (note that the metal contact schemes in the two experiments were identical). For the n-GaN, the vanadium was mostly found in a metallic state, with some VN also being found,[12] while in the case for n-AlN the converse is true. Furthermore, we find very different morphologies in the two cases—the n-GaN-based system forms a veinlike network after RTA treatment,[13] while in the n-AlN case, we observe large and small clusters. This indicates that contact formation on the (Al,Ga)N alloy system occurs differently for varying Al content. A possible explanation could be based on thermodynamic stability. The standard heat of formation ($\Delta H_{298\ K}$) for GaN, VN, and AlN is −109.7 kJ/mol, −217.3 kJ/mol, and −318.6 kJ/mol, respectively.[30] Since the heat of formation of VN is more negative than that of GaN, it is energetically more favorable to utilize a certain number of N atoms to form VN rather than GaN.

In contrast, the heat of formation of AlN is more negative than that of VN, and thus the formation of AlN is favored over that of VN in a situation where nitrogen is limited. Thus, these simple thermodynamic considerations can be one explanation for the dominant contribution of VN to the N *K* XES spectrum in the annealed n-GaN system. For the RTA-treated n-AlN system, the AlN contribution (from the substrate) dominates the nitrogen spectrum over VN, primarily due to the morphological changes discussed above. Nevertheless, VN is formed in the annealing process of AlN as well, as can be seen in the V L_3 XES spectra, which show that VN is in fact the dominant V environment in the probed volume. In order to supply sufficient energy for this (nominally) endothermic process, thermal energy is required, and thus optimal (Ohmic) metal contacts on n-AlN presumably require higher RTA temperatures than in the n-GaN case in order to form a sufficient amount (i.e., electronic pathway) of VN.

IV. SUMMARY

We have investigated the interaction between Au/V/Al/V metal contact layers and n-AlN upon annealing using a combination of spectroscopic and microscopy techniques (XES, XPS, WDS, BSE, and AFM). We have confirmed the previously speculated formation of VN as a result of the annealing step, and find significant morphological changes that lead to the formation of large and small clusters with significantly different elemental and chemical composition. Large clusters are composed of Au and an inhomogeneous distribution of V atoms in metallic and VN environments. Small clusters are composed of aluminum oxide. We have provided arguments that the nitrogen source for the VN formation is the AlN substrate and not the ambient nitrogen molecules during annealing. Finally, we have discussed the thermodynamical considerations governing the formation of GaN, VN, and AlN, and thus shed light on the metal contact interaction mechanism for the entire n-(Al,Ga)N alloy system.

ACKNOWLEDGMENTS

We gratefully acknowledge support from the U.S. Department of Energy (DOE) under Contract No. DE-FG36-05GO85032 and the Nevada System of Higher Education under SFFA Grant Nos. NSHE 07-101 and 08-03. The Advanced Light Source is supported by the Director, Office of Science, Office of Basic Energy Sciences, of the U.S. Department of Energy under Contract No. DE-AC02-05CH11231.

[1] S. Nakamura, T. Mukai, and M. Senoh, Appl. Phys. Lett. **64**, 1687 (1994).
[2] F. A. Ponce and D. P. Bour, Nature (London) **386**, 351 (1997).
[3] S. Nakamura, M. Senoh, S. Nagahama, N. Iwasa, T. Yamada, T. Matsushita, H. Kiyoku, Y. Sugimoto, T. Kozaki, H. Umemoto, M. Sano, and K. Chocho, Appl. Phys. Lett. **72**, 2014 (1998).
[4] E. Monroy, M. Hamilton, D. Walker, P. Kung, F. J. Sanchez, and M. Razeghi, Appl. Phys. Lett. **74**, 1171 (1999).
[5] C. I. Wu and A. Kahn, Appl. Surf. Sci. **162–163**, 250 (2000).
[6] J. I. Pankove and H. Schade, Appl. Phys. Lett. **25**, 53 (1974).
[7] M. C. Benjamin, C. Wang, R. F. Davis, and R. J. Nemanich, Appl. Phys. Lett. **64**, 3288 (1994).
[8] *CRC Handbook of Chemistry and Physics*, 90th ed., edited by D. R. Lide (CRC/Taylor and Francis, Boca Raton, FL, 2010).
[9] J. S. Foresi and T. D. Moustakas, Appl. Phys. Lett. **62**, 2859 (1993).
[10] K. O. Schweitz, P. K. Wang, S. E. Mohney, and D. Gotthold, Appl. Phys. Lett. **80**, 1954 (2002).
[11] R. France, T. Xu, P. Chen, R. Chandrasekaran, and T. D. Moustakas, Appl. Phys. Lett. **90**, 062115 (2007).
[12] S. Pookpanratana, R. France, M. Bär, L. Weinhardt, M. Blum, O. Fuchs, W. Yang, J. D. Denlinger, T. D. Moustakas, and C. Heske, Appl. Phys. Lett. **93**, 172106 (2008).
[13] S. Pookpanratana, R. France, M. Bär, L. Weinhardt, M. Blum, O. Fuchs, W. Yang, J. D. Denlinger, T. D. Moustakas, and C. Heske (unpublished).
[14] C. B. Stagarescu, L.-C. Duda, K. E. Smith, J. H. Guo, J. Nordgren, R. Singh, and T. D. Moustakas, Phys. Rev. B **54**, R17335 (1996).
[15] L. C. Duda, C. B. Stagarescu, J. Downes, K. E. Smith, D. Korakakis, T. D. Moustakas, J. Guo, and J. Nordgren, Phys. Rev. B **58**, 1928 (1998).
[16] M. Magnuson, M. Mattesini, C. Höglund, J. Birch, and L. Hultman, Phys. Rev. B **80**, 155105 (2009).
[17] M. Blum, L. Weinhardt, O. Fuchs, M. Bär, Y. Zhang, M. Weigand, S. Krause, S. Pookpanratana, T. Hofmann, W. Yang, J. D. Denlinger, E. Umbach, and C. Heske, Rev. Sci. Instrum. **80**, 123102 (2009).
[18] O. Fuchs, L. Weinhardt, M. Blum, M. Weigand, E. Umbach, M. Bär, C. Heske, J. Denlinger, Y.-D. Chuang, W. McKinney, Z. Hussain, E. Gullikson, M. Jones, P. Batson, B. Nelles, and R. Follath, Rev. Sci. Instrum. **80**, 063103 (2009).
[19] M. T. Anthony and M. P. Seah, Surf. Interface Anal. **6**, 107 (1984).
[20] B. L. Henke, E. M. Gullikson, and J. C. Davis, At. Data Nucl. Data Tables **54**, 181 (1993).
[21] D. W. Fischer, J. Appl. Phys. **40**, 4151 (1969).
[22] A. Callenås, L. I. Johansson, A. N. Christensen, K. Schwarz, and P. Blaha, Phys. Rev. B **32**, 575 (1985).
[23] R. Fix, R. G. Gordon, and D. M. Hoffman, Chem. Mater. **5**, 614 (1993).
[24] R. Sanjinés, P. Hones, and F. Lévy, Thin Solid Films **332**, 225 (1998).
[25] D. Briggs and M. P. Seah, *Practical Surface Analysis by Auger and X-ray Photoelectron Spectroscopy* (Wiley, New York, 1983), p. 487.
[26] A. Barrie, Chem. Phys. Lett. **19**, 109 (1973).
[27] R. Z. Bachrach, S. A. Flodström, R. S. Bauer, S. B. M. Haström, and D. J. Chadi, J. Vac. Sci. Technol. **15**, 488 (1978).
[28] A. Thompson, D. Vaughan, D. Attwood, E. Gullikson, M. Howells, K.-J. Kim, J. Kirz, J. Kortright, I. Lindau, P. Pianetta, A. Robinson, J. Underwood, G. Williams, and H. Winick, *X-ray Data Booklet* (Lawrence Berkeley National Laboratory, Berkeley, 2009), p. 15.
[29] D. N. Talwar, D. Sofranko, C. Mooney, and S. Tallo, Mater. Sci. Eng., B **90**, 269 (2002).
[30] E. A. Brandes, *Smithell's Metal Reference Book* (Butterworths, London, 1985), pp. 8-23–8-24.